

## A DETERMINATION OF THE NORTH–SOUTH HELIOSPHERIC MAGNETIC FIELD COMPONENT FROM INNER CORONA CLOSED-LOOP PROPAGATION

B. V. JACKSON<sup>1</sup>, P. P. HICK<sup>1</sup>, A. BUFFINGTON<sup>1</sup>, H.-S. YU<sup>1</sup>, M. M. BISI<sup>2</sup>, M. TOKUMARU<sup>3</sup>, AND X. ZHAO<sup>4</sup>

<sup>1</sup>Center for Astrophysics and Space Sciences, University of California, San Diego, La Jolla, CA, 92093 USA;

bvjackson@ucsd.edu, pphick@ucsd.edu, abuffington@ucsd.edu, hsyu@ucsd.edu

<sup>2</sup>RAL Space, Science and Technology Facilities Council, Rutherford Appleton Laboratory, Harwell Oxford, Didcot, Oxfordshire, OX11 0QX, UK

<sup>3</sup>Solar-Terrestrial Environment Laboratory, Nagoya University, Furo-cho, Chikusa-ku, Nagoya 464-8601 Japan

<sup>4</sup>Hansen Experimental Physics Laboratory, Stanford University, Stanford, CA, 94305 USA

*Received 2015 January 30; accepted 2015 February 27; published 2015 April 3*

### ABSTRACT

A component of the magnetic field measured in situ near the Earth in the solar wind is present from north–south fields from the low solar corona. Using the Current-sheet Source Surface model, these fields can be extrapolated upward from near the solar surface to 1 AU. Global velocities inferred from a combination of interplanetary scintillation observations matched to in situ velocities and densities provide the extrapolation to 1 AU assuming mass and mass flux conservation. The north–south field component is compared with the same ACE in situ magnetic field component—the Normal (Radial Tangential Normal) Bn coordinate—for three years throughout the solar minimum of the current solar cycle. We find a significant positive correlation throughout this period between this method of determining the Bn field compared with in situ measurements. Given this result from a study during the latest solar minimum, this indicates that a small fraction of the low-coronal Bn component flux regularly escapes from closed field regions. The prospects for Space Weather, where the knowledge of a Bz field at Earth is important for its geomagnetic field effects, is also now enhanced. This is because the Bn field provides the major portion of the Geocentric Solar Magnetospheric Bz field coordinate that couples most closely to the Earth’s geomagnetic field.

*Key words:* solar–terrestrial relations – solar wind – Sun: corona – Sun: coronal mass ejections (CMEs) – Sun: heliosphere – Sun: magnetic fields

### 1. INTRODUCTION

One of the most sought-after global heliospheric parameters is the three-dimensional (3D) magnetic field, because this field interacts with other objects imbedded in the interplanetary medium. These interactions are of primary interest in relation to Earth where, in Geocentric Solar Magnetospheric (GSM) coordinates, a southward interplanetary magnetic field component (Bz negative) can couple with the Earth’s magnetic field at the boundary of the magnetosphere, causing geomagnetic storms (e.g., Russell 2003). Motivated by earlier results indicating that the outward propagation of closed loops is observed in coronal X-ray images (Hick et al. 1995), and later results indicating that closed fields could be present from coronal mass ejections (CMEs) in the heliosphere (e.g., Hoeksema & Zhao 1992; Tokumaru et al. 2007), we began a systematic analysis to determine whether this effect could be found by applying the present UCSD modeling to this timely study.

Magnetic fields above the solar surface cannot be regularly observed at present and are often depicted by inputting the observed photospheric magnetic field into coronal magnetic field models. The potential-field source-surface model (e.g., Schatten et al. 1969; Hoeksema et al. 1983) is shown to match many aspects of the features in the lower solar corona. The current-sheet source surface (CSSS) model (Zhao & Hoeksema 1995a) more realistically determines closed and open magnetic field structures by including a description of the magnetohydrostatic equilibrium between the coronal magnetic field, the thermal pressure, and solar gravity (Bogdan & Low 1986). The CSSS model has, for instance, been shown to successfully reproduce the coronal streamer belt observed by

coronagraphs (Zhao et al. 2002) from 2.5 to 15.0 solar radii (Rs). These analyses can then be further extrapolated to give excellent comparisons with the long-term (many day) variation in the solar wind globally as shown from Ulysses observations (Zhao & Hoeksema 1995b), or near Earth (e.g., Dunn et al. 2005). The CSSS analysis has been used since 2005 to provide the background magnetic field variations on a day-by-day basis in near real time using the UCSD 3D time-dependent solar wind tomography analysis extrapolation (e.g., Jackson et al. 2013 and references therein).

Interplanetary scintillation (IPS) observations (e.g., Hewish et al. 1964) from meter-wavelength intensity variations of astronomical point-like radio sources are an important source of heliospheric remote-sensing information. These observations measure small-scale (~150 km) heliospheric density variations along each line of sight (LOS). Analyses of data from IPS have long been used to study the heliosphere (e.g., Houminer 1971; Hewish & Bravo 1986; Behannon et al. 1991; Jackson et al. 1998, 2011, 2013; Breen et al. 2008; Tokumaru 2013). The IPS normalized scintillation level (*g*-level) data serve as a proxy for density, and provide a determination of large-scale heliospheric density structures. Velocity analyses using STE-Lab data are a primary source of information about the large-scale velocities in the inner heliosphere (e.g., Tokumaru 2013). Since 1999, these data have been used to determine heliospheric structure variation on a day-by-day basis in near real time using the UCSD 3D tomography (e.g., Jackson et al. 2003, 2013 and references therein).

Here we combine these two techniques (CSSS field modeling and the velocity information gleaned from the UCSD tomography) to provide a system that allows the extrapolation upward of closed fields from near the solar surface. In these

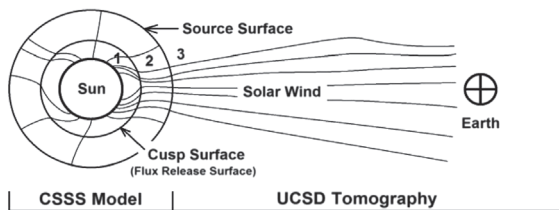


**Figure 1.** In the inner region (1), the CSSS model calculates the magnetic field using solar photospheric magnetograms. In the middle region (2), the CSSS model opens the field lines by imposing a horizontal current at the cusp surface. In the outer region (3), the UCSD 3D tomography extrapolates the magnetic field along velocity flow lines (Dunn et al. 2005).

analyses, we compare the north–south heliographic coordinate Radial Tangential Normal (RTN) field ( $B_n$ ) component extrapolated out to Earth with the same normal component determined from the *ACE* spacecraft in situ measurements (Smith et al. 1998). Section 2 gives a brief introduction to these two techniques. Section 3 presents our results to date that show high correlations from these two different data sets. We summarize in Section 4.

## 2. ANALYSIS TECHNIQUES

The Stanford CSSS model (Zhao & Hoeksema 1995a) divides the solar corona into three separate regions, each with unique physical assumptions. The underlying assumption of the CSSS model is that the interaction between solar wind plasma and the magnetic field can be more realistically recreated using three separate regions, as shown in Figure 1. The inner region is between the photosphere (first surface) and the second spherical surface. Here, the CSSS model consists of three component fields. Above this is the second or “cusp” surface that divides the inner and middle regions, and the location where a horizontal current is imposed, situated near the observed coronal cusp points. This middle region extends out to the third spherical surface. This third or “source surface”, which divides the middle and outer regions, is located near the Alfvén critical point. At this location the field component on the source surface is strictly radial. The cusp and source surfaces have been set at 1.6 and 15Rs in the current modeling. The outer region is the rest of the heliosphere, outside of the source surface, and is where the current UCSD solar wind tomographic velocity modeling can be used to extrapolate these fields outward. The original CSSS modeling, as described by Dunn et al. (2005), does not show short-term changes (several days or less) intrinsic to the solar surface, and thus discernible features from CMEs are not present in these extrapolations into the heliosphere. Also, because they are perpendicular to the solar source surface, the analysis only provides the radial ( $B_r$ ) and tangential ( $B_t$ ) components of the magnetic field caused by solar rotation in the heliosphere.

As mentioned in the introduction, outwardly projected fields using the potential field model have occasionally been thought to provide the direction of fields in the interplanetary medium at the time of CME eruptions. At and below the cusp surface, similar  $B_r$ ,  $B_t$ , and  $B_n$  component fields exist in the CSSS model as they do in the potential field model. The present analysis obtains the CSSS model  $B_n$  component of the field at the cusp surface, in this instance also termed the “flux release surface”, which is the location from which the magnetic flux escapes. It next extrapolates this flux to the

source surface and then outward to 1 AU in our modeling effort using an  $r^{-1.34 \pm 0.10}$  magnitude fall-off as shown to be present for observed Helios Bn fields in the range of 0.3–1.0 AU (Mariani & Neubauer 1990). The resulting field is finally compared with actual normal component fields observed at *ACE*. Bn fields are identically zero when using the CSSS model projection technique, since all fields at the source surface are radial.

The UCSD 3D time-dependent analysis provides a global determination of the outward solar wind velocity for use in the magnetic field extrapolations. Early considerations using IPS observations led us to develop an analysis tool that directly addresses the LOS problem for IPS measurements in order to locate heliospheric structures in 3D (Jackson et al. 1998, 2003; Jackson & Hick 2005; Jackson et al. 2010, 2011). This tool explicitly takes into account the 3D extent of heliospheric structures, including the fact that the greatest contribution is from material closest to the Sun, but without any explicit assumption about the distribution of velocity and density along these lines of sight. This analysis reconstructs 3D solar wind structures from remote-sensing data gathered from a single location in space, namely at Earth. The technique enables tapping the full IPS potential as a predictive tool for space weather purposes and, as no space-based system can, enables large and relatively inexpensive ground-based systems to be deployed for use in heliospheric research.

Transient solar wind structures such as CMEs evolve on short time scales (hours to days). For observations covering a wide range of solar elongations, heliospheric structures are viewed from different perspectives and with different LOS weighting as they move past Earth. This feature enables their time-dependent 3D reconstruction. Our present reconstruction technique incorporates a purely kinematic solar wind model. Given the velocity and density at an inner boundary source surface, a fully 3D solar wind model best fitting the observations is derived by assuming radial outflow and enforcing conservation of both mass and mass flux (Jackson et al. 1998, 2011). Best fit is achieved iteratively: when the modeled 3D solar wind at a large solar distance does not match the overall observations, the source surface values are altered to minimize the deviations. These global heliospheric analyses also iteratively match hour-averaged in situ data at Earth to provide a normalization of the two parameters that are mapped globally in the solar wind (Jackson et al. 2010, 2013).

Figure 2 is an example of the Carrington-rotation interval 2056 (CR2056) velocity at Earth from our 3D reconstruction analysis using STELab IPS data from 2007 April and May. Here we match velocities extracted from our volumetric results, with those measured by the Wind spacecraft’s in situ plasma instrument (Ogilvie & Parks 1996). The Pearson’s “ $R$ ” correlation comparison that assumes equal weighting for the IPS-extracted velocities and those measured at Wind is also shown in the right hand plot. The correlations typically have values of 0.8 or higher, and they often measure and map CME structures that last for one day or more. During this period, the *SOHO* LASCO C2 and C3 coronagraph (Brueckner et al. 1995) CDAW data center catalog (Gopalswamy et al. 2009) measures 148 CMEs. Three CMEs during this interval are partial halo events, but only one (on 2007 May 15), that is listed in the CDAW catalog associated with an NOAA GOES Space Environment Monitor satellite increase in X-rays, is likely Earth-directed. A slow CME observed in the LASCO

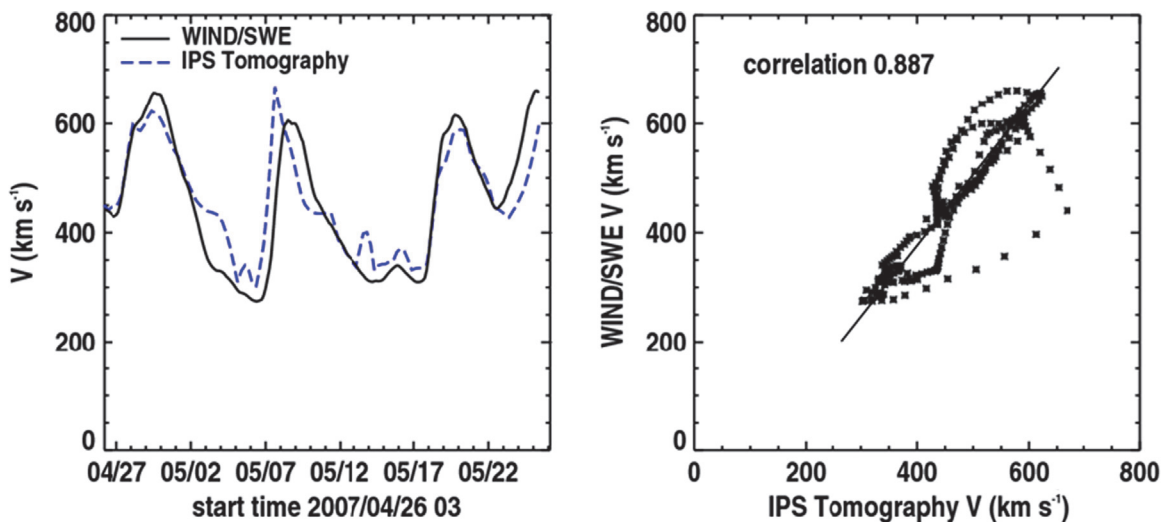


**Figure 2.** Comparison of velocity extracted from the UCSD 3D tomographic model with Wind measurements near Earth. Hourly observations by Wind are presented using a one-day boxcar average commensurate with the temporal and spatial resolutions of the tomographic model. The correlation (right panel) has been limited to the data interval shown and is presented from data points directly obtained, at a six-hour cadence, from the Wind plots.

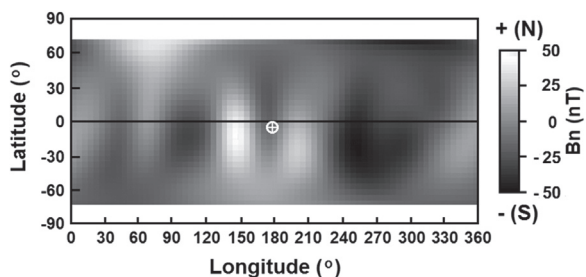


**Figure 3.** Sample of the closed field  $B_n$  component in Sun-centered Heliographic coordinates (HEEQ) for Carrington rotation 2056.152 (rotation and fraction) at the 15Rs source surface using the CSSS model. The location of the sub-Earth point is marked near the center of plot  $\sim 4^\circ$  below the heliographic equator.

coronagraph listed as a partial halo, and passing mostly to the east of the Sun–Earth line, likely arrives at Earth four to five days following and could be associated with the velocity increase measured in situ beginning on May 18. However, most of the features mapped, and especially the large excursions in velocity, are likely associated with corotating heliospheric structures.

In these analyses, velocity is an extremely important parameter to reconstruct in 3D because this can determine the propagation direction, timing, and solar origin of rapidly varying transient heliospheric structures (such as CMEs) as well as the timing of solar corotating structures. Through the fitting of our kinematic model, this allows a good determination of the solar origins of these transient structures, and their global forecast. The magnetic field is extrapolated outward from the source surface using these velocity analyses assuming the “frozen field” theorem (from Alfvén 1942).

### 3. COMPARISON RESULTS

Figure 3 shows an example of  $B_n$ , here derived at 1.6 Rs, the location of the cusp surface, and projected to 15 Rs, using an NSO SOLIS “merged” magnetogram (Keller et al. 2003). Magnetograms are obtained from this instrument once a day (in good weather); this is one of approximately 20 maps available from the SOLIS instrument throughout the course of CR2056.

This field component is traced to the 15 Rs source surface used by the tomographic model assuming an  $r^{-1.34}$  distance fall-off from Sun center, and multiplied by an arbitrary value of 0.020 to provide a slope near 1.0 for CR2056 (see Figure 4 and Section 4). The uncertainty measured in the radial fall-off observed by Helios, in turn, indicates an uncertainty in this multiplier by a factor of two. The positive and negative fields show considerable structure at this height. Each map is spline fit to form a changing field map at the UCSD tomographic model source surface where it is presented to the model at the daily cadence of the tomographic reconstruction. This field component is then extrapolated outward using the IPS tomographic velocity and again decreased by an  $r^{-1.34}$  fall-off with distance in the heliosphere.

A comparison of the  $B_n$  component extracted from the tomographic volumetric data at Earth is given in Figure 4 similar to that of velocity shown in Figure 2. The  $R = 0.614$  correlation over this interval is a typical example of most of the Carrington rotation intervals during the years 2006, 2007, and 2008. Table 1 lists the Carrington intervals studied, the correlations obtained, and the slope of the correlations using this same technique. All of the time series (from both the modeling and ACE) in these analyses contain both positive and negative excursions relative to zero. Most of the correlations are positive and some are larger than that of Figure 4. The three rotations at the beginning of each year are not shown since there are no data from the IPS arrays during these intervals. One of the Carrington rotation intervals measured had too little data (ND) from the IPS analysis to be compared. Four other rotations had only small excursions “SE” in magnetic field ( $< 0.4$  nT), and thus did not provide a meaningful  $R$  correlation. We experimented using several settings of the horizontal field extraction distance and settled for simplicity, on using the standard cusp surface distance of 1.6 Rs. Specifically, we also used 1.3Rs to provide the values shown in Table 1 (Jackson et al. 2014), and found that this did not change the correlations significantly ( $\leq 10\%$ ). This is gratifying but hardly surprising since closed flux generally has approximately the same direction whether higher or lower in the corona at the same latitude and longitude.

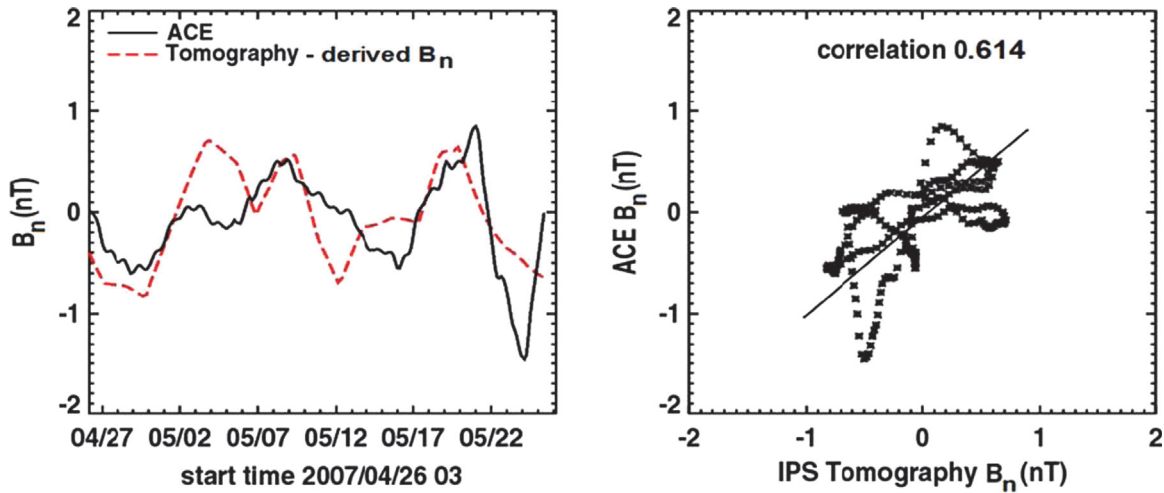


**Figure 4.**  $B_n$  component compared at Earth for CR2056. Time series over the Carrington interval are shown to the left, and a correlation comparison is made for every six hours on the right. A least squares straight line placed through the data shows the fit.

**Table 1**  
Carrington Rotations,  $B_n$  Correlations, and Slopes for Years 2006–2008

2006			2007			2008		
CR2042	ND	ND	CR2054	0.511	0.69	CR2068 <sup>a</sup>	0.634	0.84
CR2043 <sup>a</sup>	0.616	0.15	CR2055	0.558	0.80	CR2069 <sup>a</sup>	0.375	0.58
CR2044 <sup>b</sup>	0.224	0.22	CR2056 <sup>a</sup>	0.614	0.96	CR2070 <sup>a</sup>	0.589	0.94
CR2045 <sup>a</sup>	0.646	0.69	CR2057 <sup>a</sup>	0.518	0.67	CR2071	-0.318	-0.98
CR2046	0.067	0.98	CR2058	0.364	0.70	CR2072	0.029SE	1.54
CR2047 <sup>b</sup>	0.484	0.71	CR2059	0.414	0.67	CR2073	-0.073SE	-1.74
CR2048	0.721	0.30	CR2060	0.100	0.67	CR2074	0.381	2.62
CR2049 <sup>a</sup>	0.438	0.30	CR2061	0.208	0.51	CR2075	0.369	1.70
CR2050	0.505	0.34	CR2062	-0.037	-0.92	CR2076	0.382	1.31
CR2051	0.478	0.63	CR2063	0.073SE	0.80	CR2077	0.677SE	1.23

<sup>a</sup> Halo CME in interval.

<sup>b</sup> Two Halo CMEs in interval.

#### 4. SUMMARY AND CONCLUSIONS

This analysis provides a simple way to partially determine  $B_z$  at Earth since  $B_n$  is the largest contributor to this GSM coordinate that couples with the Earth’s magnetic field. Thus, this technique holds a highly significant promise for space weather forecasting.

Furthermore, while many studies in the past have suggested that the outward propagation of closed fields might serve to provide some indication of the  $B_z$  field component for CMEs (i.e., Hoeksema & Zhao 1992; Tokumaru et al. 2007), no one to our knowledge has completed a statistical study showing its application for periods near solar minimum when CMEs are mostly absent, and none using the CSSS model. The current paradigm generally presents a model that shows the solar wind flowing around closed regions of high magnetic field. Above active regions, solar wind escapes more slowly, but this flow, and also presumably the field, is assumed radial. Unexplained in this scenario is how a normal field component can be produced in the solar wind. This analysis indicates that these closed field loops are released to a significant extent in the solar wind on a regular basis and amount to a small fraction of the cusp component field. During the entire three-year period for the 25 Carrington rotations studied here with valid correlations,

there are only 12 partial halo CMEs listed in the CDAW CME catalog that were judged to be Earth-directed. There is a tendency for these 12 (9 as opposed to 3) to be associated with Carrington rotations with a correlation greater than the mean value of 0.382. However, this association is present with such a sparse number of CMEs that its significance is questionable for events that, at most, last only a few days during any one Carrington rotation.

We note that the current fraction of the calculated horizontal field magnitude that makes it into the solar wind is somewhat arbitrary. Additionally, the radial fall-off has not been observed below 0.3 AU, and is assumed to be the same as it is between 0.3 and 1.0 AU. To extrapolate this field outward and get the desired one-to-one correlation for CR2056, we set the portion of the field that escapes to the solar wind at a value of 0.02 (that is, 2% of the calculated value of the field). This fractional amount of flux that has escaped can be further refined by, for instance, averaging the slopes of all the Carrington rotations with mean correlation values greater than 0.382. The mean of the slopes for this well-correlated distribution is 0.621, and thus on average the escaped flux is somewhat lower, with a fractional value of about 0.0124, again with a potential error of at least a factor of two due to the uncertainties in the slope of

the radial fall-off and large range in the slope values as noted before.

This amount must surely have something to do with the physics behind the escape of the field from closed regions and, furthermore, is likely not constant everywhere in the corona. Especially during CMEs, the presence of this horizontal field could be greatly changed at its source; this provides part of the motivation for our present analysis to be at a time when CMEs are mostly absent. With CMEs present, the field extrapolated outward from the surface must also undergo change during its transit in ways not governed by the simple physics (preserving mass and mass flux) implicit in our current kinematic modeling. To work best, physics that includes magnetic field effects will also play a role, and thus 3D-MHD analyses could provide a better approximation of the field propagation into the inner heliosphere from this effect.

To provide a robust solar wind forecast, contaminant data glitches that sometimes spoil the analysis need to be identified, and if possible remedied in an automatic fashion. Thus far, these analyses have not been used (as noted) to provide the fraction of a day short-term variations that are present from rapidly changing transients (CMEs) even though this was the original intent of these analyses. Further work on more short-term magnetic field component extrapolation is currently underway.

This work is expected to continue in several ways. The amplitude of the effect needs to be further adjusted statistically to give the best general in situ results from the constraints imposed by each analysis technique. We found that the best correlations shown are somewhat enhanced when a delay of about one day is imposed in the progression outward from the solar surface to the source surface, and we adopted this delay throughout this study to provide the correlations presented. This also needs a more careful exploration, especially when higher-resolution tomographic analyses are used, different heliospheric structures are studied, or when 3D-MHD analyses are incorporated. Finally, a classification of each of the various known features observed remotely and in situ is important in order to ascertain the differences between corotating and transient structures. The research aspect of separating these analyses requires a better understanding of our assumptions for near the solar surface and may require the incorporation of the non-radial expansion of the field there. Near solar observations of this effect in X-rays using data from the Yohkoh spacecraft have been available since those of Hick et al. (1995), and require the best performance from current imaging facilities; these images generally only infer surface fields and give little indication of the field magnitude or sign.

B.V.J., P.P.H., and H.-S.Y. acknowledge partial support for this effort from NSF contract AGS-1358399 and NASA

contract NNX14AC11G to the University of California, San Diego. M.M.B. acknowledges support via the IHR grant and Core Space Weather funding from the Science and Technology Facilities Council (STFC) to RAL Space. The IPS observations were carried out under the solar wind program of the Solar-Terrestrial Environment Laboratory (STELab) of Nagoya University.

## REFERENCES

- Alfvén, H. 1942, *Natur*, 150, 405  
 Behannon, K. W., Burlaga, L. F., & Hewish, A. 1991, *JGR*, 96, 21213  
 Bogdan, T. J., & Low, B. C. 1986, *ApJ*, 306, 271  
 Breen, A. R., Fallows, R. A., Bisi, M. M., et al. 2008, *ApJL*, 683, L79  
 Brueckner, G. E., Howard, R. A., Koomen, M. J., et al. 1995, *SoPh*, 162, 357  
 Dunn, T., Jackson, B. V., Hick, P. P., Buffington, A., & Zhao, X. P. 2005, *SoPh*, 227, 339  
 Gopalswamy, N., Yashiro, S., Michalek, G., et al. 2009, *EM&P*, 104, 295  
 Hewish, A., & Bravo, S. 1986, *SoPh*, 106, 185  
 Hewish, A., Scott, P. F., & Wills, D. 1964, *Natur*, 203, 1214  
 Hick, P. P., Jackson, B. V., Rappoport, S., et al. 1995, *GeoRL*, 22, 643  
 Hoeksema, J. T., & Zhao, X. 1992, *JGR*, 97, 3151  
 Hoeksema, J. T., Wilcox, J. M., & Scherrer, P. H. 1983, *JGR*, 88, 9910  
 Houminer, Z. 1971, *NPhS*, 231, 165  
 Jackson, B. V., & Hick, P. P. 2005, in *Astrophysics and Space Science Library*, Vol. 314, *Solar and Space Weather Radiophysics, Current Status and Future Developments*, ed. D. E. Gary, & C. U. Keller (Dordrecht: Kluwer), 355  
 Jackson, B. V., Hick, P. L., Kojima, M., & Yokobe, A. 1998, *JGR*, 103, 12049  
 Jackson, B. V., Hick, P. P., Buffington, A., et al. 2003, in *Solar Wind Ten AIP Conf. Proc.* 679, *Time-dependent Tomography of Heliospheric Features Using Interplanetary Scintillation (IPS) Remote-sensing Observations*, ed. M. Velli, R. Bruno, & F. Malara (Melville, NY: AIP), 75  
 Jackson, B. V., Hick, P. P., Bisi, M. M., Clover, J. M., & Buffington, A. 2010, *SoPh*, 265, 245  
 Jackson, B. V., Hick, P. P., Buffington, A., et al. 2011, *JASTP*, 73, 1214  
 Jackson, B. V., Hick, P. P., Bisi, M. M., Clover, J. M., & Buffington, A. 2013, *SoPh*, 285, 151  
 Jackson, B. V., Yu, H.-S., Hick, P., et al. 2014, *Using IPS Magnetic Modeling to Determine Negative Bz*, Abstract SH21C-4144 presented at the AGU Fall Meeting (Washington, DC: AGU)  
 Keller, C. U., Harvey, J. W., & Giampapa, M. S. & The SOLIS Team 2003, *Proc. SPIE*, 4853, 194  
 Mariani, F., & Neubauer, F. M. 1990, in *The Interplanetary Magnetic Field*, Vol. 20, ed. M. C. E. Huber, L. J. Lanzerotti, & D. Stoffler (Berlin: Springer-Verlag), 183  
 Ogilvie, K. W., & Parks, G. K. 1996, *GeoRL*, 23, 1179  
 Russell, C. T. 2001, in *Space Weather Geophys. Mono. Series*, Vol. 125, *Solar Wind and Interplanetary Magnetic Field: A Tutorial*, ed. P. Song, H. J. Singer, & G. L. Siscoe (Washington, DC: AGU), 73  
 Schatten, K. H., Wilcox, J. W., & Ness, N. E. 1969, *SoPh*, 6, 442  
 Smith, C. W., L'Heureux, J., Ness, N. F., et al. 1998, *SSRv*, 86, 613  
 Tokumaru, M. 2013, *Proc. Japan Acad.*, Ser. B, 89, 67  
 Tokumaru, M., Kojima, M., Fujiki, K., Yamashita, M., & Jackson, B. V. 2007, *JGR*, 112, A05106  
 Zhao, X. P., & Hoeksema, J. T. 1995a, *JGR*, 100, 19  
 Zhao, X. P., & Hoeksema, J. T. 1995b, *AdSpR*, 16, 181  
 Zhao, X. P., Hoeksema, J. T., & Rich, N. B. 2002, *AdSpR*, 29, 411